Accepted Manuscript

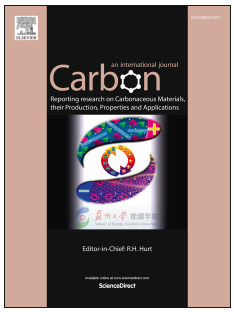

Reduction-oxidation dynamics of oxidized graphene: Functional group composition dependent path to reduction

Yi-Zhe Hong, Hung-Chieh Tsai, Yu-Han Wang, Jukka Aumanen, Pasi Myllyperkiö, Andreas Johansson, Yen-Chien Kuo, Lo-Yueh Chang, Chia-Hao Chen, Mika Pettersson, Wei-Yen Woon

PII: S0008-6223(17)31280-0

DOI: 10.1016/j.carbon.2017.12.047

Reference: CARBON 12677

To appear in: *Carbon*

Received Date: 5 October 2017

Revised Date: 5 December 2017

Accepted Date: 12 December 2017

Please cite this article as: Y.-Z. Hong, H.-C. Tsai, Y.-H. Wang, J. Aumanen, P. Myllyperkiö, A. Johansson, Y.-C. Kuo, L.-Y. Chang, C.-H. Chen, M. Pettersson, W.-Y. Woon, Reduction-oxidation dynamics of oxidized graphene: Functional group composition dependent path to reduction, *Carbon* (2018), doi: 10.1016/j.carbon.2017.12.047.

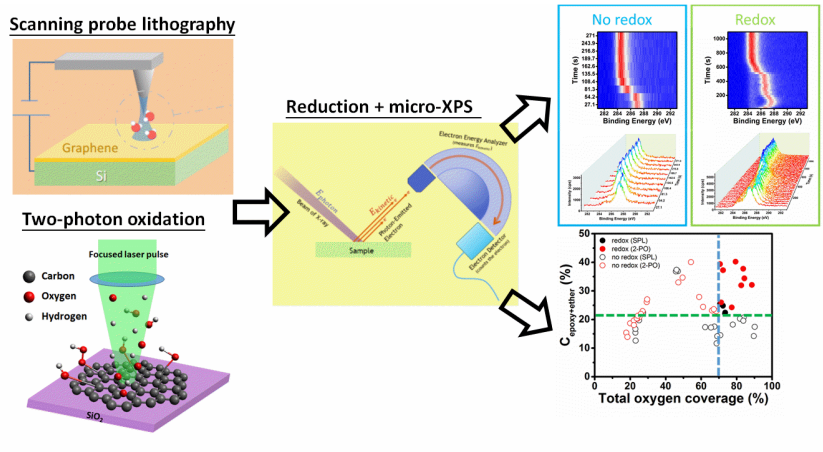

Reduction-oxidation dynamics of oxidized graphene: Functional group composition dependent path to reduction

Yi-Zhe Hong[1+], Hung-Chieh Tsai[1+], Yu-Han Wang[1], Jukka Aumanen[2], Pasi Myllyperkiö[2], Andreas Johansson[2,3], Yen-Chien Kuo[4], Lo-Yueh Chang[4], Chia-Hao Chen[4], Mika Pettersson[2], Wei-Yen Woon[1*].*

[1]Department of Physics, National Central University, Jungli, 32054, Taiwan, Republic of China

[2]Nanoscience Center, Department of Chemistry, P.O. Box 35, FI-40014, University of Jyväskylä, Finland

[3]Nanoscience Center, Department of Physics, P.O. Box 35, FI-40014, University of Jyväskylä, Finland

[4]National Synchrotron Radiation Research Center, Hsinchu, 30076, Taiwan, Republic of China

ABSTRACT

Micrometer-sized oxidation patterns containing varying composition of functional groups including epoxy, ether, hydroxyl, carbonyl, carboxyl, were created in chemical vapor deposition grown graphene through scanning probe lithography and pulsed laser two-photon oxidation. The oxidized graphene films were then reduced by a focused x-ray beam. Through in-situ x-ray photoelectron spectroscopy measurement, we found that the path to complete reduction depends critically on the total oxygen coverage and concentration of epoxy and ether groups. Over the threshold concentrations, a complex reduction-oxidation process involving conversion of functional groups of lower binding energy to higher binding energy is observed. The experimental observation is discussed and compared to previous work on reduced graphene oxide.

*Corresponding author. E-mail: wywoon@phy.ncu.edu.tw; mika.j.pettersson@jyu.fi

[+]These author contributed equally to this work

1. Introduction

Since the discovery of various 2D materials including graphene and transition metal dichalcogenides, tremendous scientific progresses have been made. There are high expectations for the applications of 2D materials in electronics, optics, and many other fields [1-3]. However, true realization of the anticipated applications remains limited due to cost and stability issues. Graphene Oxide (GO) is one of the most widely applicable 2D materials in industry nowadays [4-7]. Through oxidizing graphite with strong oxidizing agent, separation of hydrophilic graphene sheets containing oxygenated functionalities can be achieved in large scale and with relatively low cost [8,9]. The composition of functional groups in GO is highly dependent on the preparation protocols and control of environment [10]. Furthermore, due to the disruption of sp^2 configuration by the presence of the functional groups, the electrical and thermal conductivities of GO are usually not good. To improve the electrical and thermal properties, reduction of GO to render reduced graphene oxide (rGO) is necessary [11]. Compared to any other preparation methods, reduction of GO is the most economical way to obtain conductive graphene based 2D materials.

Nevertheless, due to complexity in the composition of functional groups, the physicochemical process involved in GO reduction process is not fully understood.

Mattevi et al. reported evolution of electrical, chemical and structural properties of thermally reduced GO thin film [12]. They concluded that sp^3 bonds formed between carbon atoms and residual oxygen in the basal plane are the major hindrance for complete reduction of GO back to high mobility graphene. Larciprete et al. reported that epoxy-epoxy recombination or epoxy-ether interaction is highly dependent on the initial concentration of oxide functional groups during the reduction process [13]. Eigler et al. reported the formation and decomposition of intercalated CO_2 in thermal reduction of GO. With increasing temperature, the CO_2 blisters form at the surface of GO. Eventually vacancies are formed on the rGO sheets after volatile desorption [14]. Moreover, GO is found to be an unstable material in which complex chemical reactions such as reduction-oxidation (redox), could occur at room temperature [15]. In a redox process, the conversion of epoxy group to carbonyl and carboxyl are dominant at the beginning of reduction, followed by gradual decrease in concentration of C-O related functional groups in the later stages. The complex redox process could consume carbon atoms in the graphene network through release of CO/CO_2 mixtures, thereby disrupt the graphene network, and result in incomplete reduction and degradation in electrical conductivity. In fact, some low energy input provided from characterization processes such as x-ray photoelectron (XPS) or micro-Raman spectroscopies are found to be enough to unintentionally change the initial properties

of GO [16]. The above observations suggest that the eventual chemical and structural properties of rGO are highly susceptible to variation in the reduction processes. So far, there were not many systematic and quantitative investigations on the reduction dynamics due to difficulty in controlling the initial conditions of GO and lack of in situ characterization tools.

Most graphene oxidation methods including thermal or chemical oxidations involve formation of oxide functional groups in graphene network without the ability to locally control the extent of oxidation. In particular, the chemical composition and concentration of oxide functional groups may not be uniformly distributed in a GO sheet. From our experience, we found that the local tribological, structural and chemical characteristics of a chemical vapor deposition (CVD) grown graphene can vary from point to point in the same sample. The dynamics of defect generation and its reduction may depends on the initial condition of local environment, namely the local structural and chemical conditions of the graphene crystal. It is therefore intriguing to investigate the defect generation and reduction dynamics of locally oxidized regions in a vastly different initial local environment.

Here we present a systematic, in-situ study on the reduction dynamics of graphene containing controlled amount of oxygenated functionalities. Two different methods , scanning probe lithography (SPL), an atomic force microscopy (AFM) based

technique, and two-photon oxidation (2-PO), a laser based technique, have been employed to prepare oxidized graphene with different total oxygen coverage (TOC) up to 85 %. Commonly found functional groups in GO including epoxy, ether, hydroxyl (C-OH), carbonyl (C=O), and carboxyl (COOH) are found in the oxidized graphene. We found a critical epoxy and ether concentration that determines the route to complete reduction. Similar redox dynamics akin to the one observed in GO reduction is characterized and analyzed. Additionally, it is found that the redox dynamics for the oxidized graphene prepared by two vastly different methods share similarity.

2. Experiment

2.1 Sample preparation

Graphene sample preparation. Two sources of graphene were used. First, we purchased a silicon chip with 300 nm SiO_2 and a monolayer of CVD-grown graphene from Graphenea Inc. Using electron beam lithography and PMMA, a reference grid was patterned, with lines that were 1 μm wide and that defined a 10 x 10 matrix of squares, each 200 μm by 200 μm in size. Reactive ion etching was used to remove graphene from the bottom of the pattern before it was metallized using 2 nm Ti as adhesion layer and 30 nm Au on top. The chip was covered with an additional PMMA layer as protection, and then diced to a suitable size of 5 mm by 5 mm, before finalizing the patterning with lift-off procedure. The resulting reference grid allowed positioning of the 2-PO and SPL patterns at a known location so that they could be found during characterization measurements. All 2-PO oxidized

graphene were prepared on this sample at the University of Jyväskylä, Finland, while some SPL oxidized graphene were prepared on this sample at the National Central University, Taiwan. The second source of graphene samples came from our custom made rapid thermal chemical vapor deposition (RTCVD) system. Details of the RTCVD growth can be found in our previous work [17]. The graphene film was grown on Cu foil at 1000 ℃ with CH_4/H_2 ratio of 1:2 (H_2 100 sccm, CH_4 50 sccm) under low pressure (1.5 Torr). The as-grown graphene was transferred to a 300 nm SiO_2/Si wafer using standard wet processing involving PMMA and bubble generation through NaOH electrolysis [18]. Silver paint (Ted Pella) wires were drawn on the surface and connected to the backside of the sample as grounding and marker for pattern location. Most of the SPL oxidized graphene were prepared on this sample. The quality of the two types of graphene was checked by micro-Raman spectroscopy. For both samples, negligible D band was found and the samples were mostly covered with single layer graphene (symmetric 2D and $I_{2D}/I_G > 2$). The Raman spectroscopies of the initial conditions are listed in supplementary materials.

Scanning probe lithography. SPL was conducted with a Bruker Innova AFM using a conductive AFM probe (Pt/Ir coated point-probe series, Nanosensor) at room temperature in a sealed humidity controlled chamber. A custom implemented external bias source allowed for bias application. Square patterns of about 1.5μm x 1.5 μm were drawn by using the built-in software (Nanoplot, Bruker) with closed loop function to enable exact positioning down to nanometer scale precision. In this work, we applied voltage biases ($|V_{bias}|$) from 7 V to 10 V. More details of the SPL method can be found in our previous publication [19]

Two photon oxidation. Photon-oxidation of the graphene sample was performed by using the output beams of two non-collinear optical parametric amplifiers (NOPAs,

Orpheus-N, Light Conversion) that were pumped with an amplified femtosecond laser (Pharos-10, 600 kHz, Light Conversion) through a high numeric aperture microscope objective (Nikon LU Plan ELWD 100x/0.80). Detailed description of the laser setup can be found from our previous work [20]. Oxidations were carried out under ambient air using one laser beam containing 540 nm laser pulses of 40 fs pulse duration, 13 pJ pulse energy and 600 kHz repetition rate. Oxidation patterns were formed by moving the sample with a XYZ piezo scanner in 100 nm steps to produce 2 x 2 μm^2 oxidized areas i.e. each of the squares consists of 400 oxidation spots partially overlapping each other. The exposure times (T_{ox}) for oxidation were 0.1 to 2.0 s/spot.

2.2 Characterization

Optical images (OM) were acquired through an upright microscope (BX-51, Olympus). Topographical and lateral force information (LFM) were acquired through AFM. The chemical bond profile was probed with micro-photoelectron spectroscopy (μ-XPS) through soft x-ray emission from a synchrotron radiation facility (beam line 09A1, National synchrotron radiation research center, Hsinchu). Chemical bonds associated with modification of the sp^2 bond and functionalization of carbon were identified by taking the carbon 1s spectra around photoelectron energy at 284.5 eV (supplementary materials) [21]. By focusing the intense x-ray beam down to < 0.1 um by a zone plate, and scanning the sample with a motorized stage, the chemical bond profile of the SPL defects was obtained with sub-micrometer resolution [22]. While the x-rays involved in taking the spectrum did not change the spectrum of the pristine graphene, repeated exposure of the SPL/2-PO treated samples resulted in significant changes in the C1s spectra after each round (20s) of acquisition. Thus only the first spectrum taken at each point was

used to represent initial chemical bonding condition of SPL/2-PO treated patterns prior to reduction. The XPS signal collected from each scanned spot was used to produce chemical mapping images (scanning photoelectron microscopy, SPEM). Reduction of oxidized graphene occurs with prolonged irradiation of focused x-ray on the oxidized patterns. The reduction dynamics was recorded *in-situ* by taking multiple high resolution C1s XPS (acquisition time = 20s) with continuous x-ray irradiation at target spots until the XPS remained unchanged (located according to the contrast shown in SPEM acquired immediately prior to high resolution XPS acquisition). The reduction was probably caused by bombardment from low energy photo-electrons generated from both graphene and the underneath SiO_2 by the absorption of x-ray radiation.

3. Results

Figure 1 shows the OM, LFM, and SPEM images (from left to right) of (a) SPL and (b) 2-PO patterns prepared with various experimental conditions, each indicated in the figure. For both SPL and 2-PO patterns, the oxidized areas appear optically brighter than the pristine graphene, probably due to difference in interference. Contrast is found in LFM as friction is higher in the oxidized patterns due to the increased roughness. SPEM images shown in C1s (284.5 eV) channel show that C=C bond concentration is lower in the oxidized areas. The above observations suggest the optical, tribological, and chemical properties of SPL and 2-PO oxidized graphene are similar under certain parameter sets [23, 24]. For example, at $|V_{bias}| = 7$ V, and $T_{ox} = 0.5$ s, the chemical compositions are almost identical (supplementary materials).

However, at T_{ox} = 2.0 s, the C=C bond concentration is very low, while SPL oxidized graphene always retain some C=C bonds even at the highest achievable $|V_{bias}|$ (otherwise the AFM tip will be damaged). Overall speaking it shows that 2-PO oxidation offer wider tunability of TOC than SPL. Another point to note is that applying the same SPL $|V_{bias}|$ on two different graphene samples may result in different retained TOC or composition of functional groups, probably due to difference in the local structural conditions, as accounted in our previous publication [23]. Nevertheless, as we are focusing on the reduction-oxidation dynamics, we can treat those variations as oxidized graphene with different initial conditions.

Figs. 2(a), 2(b) and 2(c) show the typical *in-situ* acquired μ-XPS contour plots and waterfall spectra measured at oxidized patterns prepared under two different conditions. Three catergories of reduction behaviors are found. (A) No redox cases: low SPL $|V_{bias}|$ (7 V, 8 V) or short T_{ox} (0.1, 0.2, 0.3, 0.4, 0.5 s/spot), (B) Border-line cases: high SPL $|V_{bias}|$ (9 V, 10 V) or medium T_{ox} (0.6, 0.8 s/spot), and (C) Redox cases: long T_{ox} (1.0, 1.5 s, 2.0 s/spot), respectively. For category A, the initial TOC is < 60 % and the spectrum shows a monotonic trend in conversion of functional groups from higher binding energy (B.E.) (carbonyl, carboxyl) (B.E. > 287 eV) to lower B.E. (ether and epoxy) (B.E. < 287 eV). For category C, the initial TOC is 78~90 %, and a redox behavior in which conversion of epoxy and ether groups to carbonyl are

observed in the beginning of x-ray exposure process, followed by a step-by step reduction process that eventually leads to complete conversion to C=C bonds. For all category C cases prepared by 2-PO oxidation where TOC are higher than 78 %, redox dynamics are always found. On the other hand, category B possesses wide range distribution of TOC from 60 % to 90 %, and its reduction dynamics belongs to a border like case in which redox may or may not occur. It seems like TOC alone is not enough for prediction of redox behavior, i.e., there may be other criterion that needs to be fulfilled in order to have redox dynamics.

The detailed chemical composition of oxidized graphene prepared under various conditions, and the temporal evoultion of each oxide functional group due to reduction, are presented in Fig. 3. The preparation condition and the TOC of each oxidized graphene is listed as follows: (a) Graphenea graphene, SPL $|V_{bias}|$ = 10 V, TOC = 70.7 %; (b) Graphenea graphene, 2-PO T_{ox} = 0.6 s/spot, TOC = 68.5 %; (c) RTCVD graphene, SPL $|V_{bias}|$ = 10 V, TOC = 89. 7 %; and (d) Graphenea graphene, 2-PO T_{ox} = 1.0 s/spot, TOC = 88.6 %. Comparing the temporal evolution plots in Figs. 3(a) and 3(b), we can see that redox dynamics (whereas ether and epoxy groups decrease, while carbonyl and carboxyl increases) only occur for the higher TOC case in Fig. 3(a). For the lower TOC case in Fig. 3(b), the temporal evolution shows that the ether and epoxy groups monotonically increase, while the carbonyl and carboxyl

monotonically decreases. Despite the difference in the early stage of reduction, most of the oxide functional groups were converted to C-C+C=C bonds eventually (> 80 %), with some remaining C-OH, similar to what was found in our previous work [22-24]. On the other hand, comparing the two very high TOC (88~89 %) cases in Figs. 3(c) and 3(d), redox can be found only in (d). A closer look at the composition of functional groups in the oxidized graphene reveals that the overall compositions are different in these samples. In particular, the concentration of ether and epoxy ($C_{ether+epoxy}$) are different among the four samples in Fig. 3. In (a), (b), (c), and (d), $C_{ether+epoxy}$ is 25.5 %, 22.9 %, 14.2 %, and 32.1 %, respectively. The above observations show that despite having similarly high TOC in both (c) and (d), redox dynamics only occur when $C_{ether+epoxy}$ is higher. On the other hand, by comparing case (a) and (b), we can see that despite they both have $C_{ether+epoxy}$ > 22 %, no redox can be observed as TOC is lower in (b). The above observations suggest there may be a threshold TOC and $C_{ether+epoxy}$ for the occurenece of redox.

In light of the above observations, we plot the statistical diagrams in Fig. 4, including all available data (as shown in the scattered points in Figs. 4(a) to 4(d)), to correlate the redox behavior to composition of functional groups. As shown in Fig. 4(a), redox is more likely as $C_{C=C+C-C}$ decreases ($C_{C=C+C-C}$ decreases monotonically as TOC increases, understandably). However, there are still some no-redox cases in the

low $C_{C=C+C-C}$ regime, indicating that loss of integrity of the sp^2 carbon network is not the key for redox occurrence. Figs. 4(b) and 4(c) show the correlation plots for TOC vs. concentration of functional groups with lower B.E.s ($C_{epoxy+ether+hydroxyl}$, B.E. < 287 eV) and, higher B.E.s ($C_{C=O+COOH}$, B.E. < 287 eV), respectively. In both plots, there is no clear indication for a critical threshold strongly correlated to TOC. On the other hand, in Fig. 4(d) we can clearly see that criteria for redox to occur are two-fold. First a high enough TOC (> 70 %), second a high enough $C_{ether+epoxy}$ (> 22 %) are concurrently needed to enable redox.

4. Discussion

In Matsumoto et al., ultra violet (UV) photo-reduction of GO was investigated [25]. They found decrease of C-O related bonds with concurrent increase of C-C related bonds after UV photo-reduction for several hours. The final A_{C-O}/A_{CC} (XPS peak area of C-O related bonds divided by XPS peak area of C-C related bonds) is about 0.2. While in Prezioso et al. [26], the photo-reduction by extreme-UV and soft x-ray irradiation (not as tightly focused as in our case) resulted in 0.6 I_{C-O}/I_{C-SP^2} (XPS intensity of C-O related bonds/ XPS intensity of SP^2 C-C bonds). Both works reported on photo-reduction and discussed in depth on the reduction mechanisms. Nevertheless, the detailed inter-relationship between time evolution of each functional groups are not reported in the above works. In our work, we focus on the detailed time evolution

of each bonds, and found a complex redox dynamics may occur under high TOC. Furthermore, probably due to the nature of tightly focused x-ray, we are able to observe more complete reduction of graphene. In many cases in our study, x-ray irradiation induced reduction can result in ~ 90 % of reduction to C-C and C=C bonds.

Understanding the above observations may require further theoretical calculations such as density functional theory (DFT) or molecular dynamics (MD) simulations. We lack the theoretical support in this work but some insight can be gained from previous work on thermal reduction of GO. Larciprete et al. [27] showed experimentally and theoretically that the path for reduction depends on surface density of TOC. For low TOC the predominant path for reduction is through the epoxy diffusion-clustering-recombination pathway, with release of molecular oxygen, and the carbon network remains intact. In this scenario, functional groups with higher B.E. such as carbonyl or carboxyl may be first reduced back to functional groups with lower B.E. such as epoxy or ether, before material is fully reduced back to oxygen free graphene, following the above pathway. On the other hand, under high TOC, interaction between epoxy-ether or epoxy-epoxy could lead to GO reduction through the pathway of lactone-semiquinone, and then lactone-ether precursor, along with release of CO_2 or CO, leaving the carbon network disrupted due to generation of

vacancies. The dangling bonds around the defects and vacancies could become active sites for oxygen gas absorption and chemical reactions between the oxygen and carbon atoms. With continuous energy input (such as the one provided by x-ray induced photoelectron in this work), oxidation reactions to form functional groups with higher B.E. could occur. Usually, for thermal reduction or UV photo-reduction of GO, the reduction ends at the point where carbon network is disrupted and complex functional group clusters are generated. The residual TOC remains relatively high because epoxy diffusion become less probable to promote further reduction through the first pathway described above. As shown in Fig. 5(a), the final concentration of C-C and C=C bonds ($C_{C\text{-}C+C=C}$) tends to be lower as $C_{epoxy+ether}$ is higher. On the other hand, there seems to be weaker correlation between $C_{C\text{-}C+C=C}$ and TOC (Fig. 5(b)). Moreover, lower final $C_{C\text{-}C+C=C}$ is found for most of the redox cases (marked as full symbols). Nevertheless, contrary to previous works, the $C_{C\text{-}C+C=C}$ in our work can be as high as ~ 90 % even for some high TOC and $C_{epoxy+ether}$ cases, probably because the x-ray induced photoelectron bombardment can still enable epoxy evolution even when the carbon network is disrupted. The above physical pictures are depicted in the diagrams in Fig. 5(c). In short, our experimental result can be well described within the framework of Larciprete et al. [27], but there is additional information revealed in this work, in which conversion between functional groups are measured in more detail,

so that it is shown that even under high TOC, redox can only occur when there is proper composition of functional groups (high $C_{epoxy+ether}$). Furthermore we show that almost complete deoxygenation is possible through reduction by x-ray induced photoelectron, even when TOC is high.

Conclusion

In summary, we performed a systematic, *in-situ* investigation on the reduction-oxidation dynamics of micrometer-sized oxidized graphene areas through x-ray irradiation. Oxidized graphene containing functional groups including epoxy, ether, hydroxyl, carbonyl, carboxyl, were created in CVD grown graphene through SPL and 2-PO. Through *in-situ* XPS measurements, we found that the paths for complete reduction are critically dependent on both TOC and $C_{epoxy+ether}$. Over a threshold TOC and $C_{epoxy+ether}$, a complex redox process in which conversion of epoxy and ether groups to carbonyl and carboxyl is dominant at the beginning of x-ray irradiation process, followed by a step-by step reduction process that eventually leads to conversion to c-C and C=C bonds. On the other hand, below the threshold TOC and $C_{epoxy+ether}$, the reduction dynamics follows the step-by-step process whereas oxide groups with higher B.E.s are sequentially reduced to those with lower B.E.s.

Acknowledgement

This work is supported by the Ministry of Science and Technology of the Republic of China under contract MOST106-2112-M008-003-MY3

REFERENCES

1. A. K. Geim, K. S. Novoselov, The rise of graphene. Nature Mater. 6 (2007), 183-191.
2. Y. Zhu, S. Murali, W. Cai, X. Li, S. W. Ji, J. R. Potts, et al., Graphene and graphene oxide: synthesis, properties, and applications. Adv. Mater. 22 (2012), 3906-3924.
3. Q. H. Wang, K. Kalantar-Zadeh, A. Kis, J. N. Coleman, M. S. Strano, Electronics and optoelectronics of two-dimensional transition metal dichalcogenides. Nature Nanotechnol. 7 (2012), 699-712.
4. D. Chen, H. Feng, J. Li. Graphene oxide: preparation, functionalization, and electrochemical applications. Chem. Rev. 112 (2012), 6027-6053.
5. Y. Wang, Z. Shi, Y. Huang, Y. Ma, C. Wang, M. Chen, et al., Supercapacitor devices based on graphene materials. J. Phys. Chem. C. 113 (2009), 13103-13107.
6. H. Y. Jeong, J. Y. Kim, J. W. Kim, J. O. Hwang, J.E. Kim, J. Y. Lee, et al., Graphene oxide thin films for flexible nonvolatile memory applications. Nano Lett. 10 (2010), 4381-4386.

7. F. Wang, S. B. Singh, M. V. Limaye, Y. C. Shao, S. H. Hsieh, L. Y. Chen, et al. Visualizing chemical states and defects induced magnetism of graphene oxide by spatially-resolved-X-ray microscopy and spectroscopy. Sci. Rep. 5 (2015), 8448.
8. W. S. Hummers, R. E. Offeman, Preparation of graphitic oxide. J. Am. Chem. Soc. 80 (1958), 1339.
9. D. Li, M. B. Müller, S. Gilje, R. B. Kaner, G. G. Wallace, Processable aqueous dispersions of graphene nanosheets. Nature Nanotechnol. 3 (2008), 101-105.
10. N. Morimoto, T. Kubo, Y. Nishina, Tailoring the oxygen content of graphite and reduced graphene oxide for specific applications. Sci. Rep. 6 (2016), 21715.
11. G. Eda, G. Fanchini, M. Chhowalla, Large-area ultrathin films of reduced graphene oxide as a transparent and flexible electronic material. Nature Nanotechnol. 3 (2008), 270-274.
12. C. Mattevi, G. Eda, S. Agnoli, S. Miller, K. A. Mkhoyan, O. Celik, et al., Evolution of electrical, chemical, and structural properties of transparent and conducting chemically derived graphene thin films. Adv. Funct. Mater. 19 (2009), 2577.
13. R. Larciprete, P. Lacovig, S. Gardonio, A. Baraldi, S. Lizzit, Atomic oxygen on graphite: chemical characterization and thermal reduction. J. Phys. Chem. C. 116 (2012), 9900-9908.

14. S. Eigler, C. Dotzer, A. Hirsch, M. Enzelberger, P. Müller, Formation and decomposition of CO_2 intercalated graphene oxide. Chem.Mater. 24 (2012), 1276-1282.

15. D. N. Voylov, I. N. Ivanov, V. I. Bykov, S. B. Tsybenova, I. A. Merkulov, S. A. Kurochkin, et al., Oscillatory behaviour of the surface reduction process of multilayer graphene oxide at room temperature, RSC Adv. 6 (2016), 78194.

16. M. Rogala, P. Dabrowski, P. J. Kowalczyk, I. Wlasny, W. Kozlowski, A. Busiakiewicz, et al., The observer effect in graphene oxide–How the standard measurements affect the chemical and electronic structure. Carbon 103 (2016), 235-241.

17. M. C. Chuang, W.-Y. Woon. Nucleation and growth dynamics of graphene on oxygen exposed copper substrate. Carbon 103 (2016), 384-390.

18. Y. Wang, Y. Zheng, X. Xu, E. Dubuisson, Q. Bao, J. Lu, et al., Electrochemical delamination of CVD-grown graphene film: toward the recyclable use of copper catalyst. ACS Nano 5 (2011), 9927-9933.

19. H. M. Chien, M. C. Chuang, H. C. Tsai, H. W. Shiu, L. Y. Chang, C. H. Chen, et al., On the nature of defects created on graphene by scanning probe lithography under ambient conditions. Carbon 80 (2014), 318-324.

20. J. Aumanen, A. Johansson, J. Koivistoinen, P. Myllyperkiö, and M. Pettersson, M. Patterning and tuning of electrical and optical properties of graphene by laser induced two-photon oxidation. Nanoscale 7 (2015), 2851-2855.

21. D. Briggs, G. Beamson, High resolution XPS of organic polymers: The scienta ESCA300 database appendix I (John Wiley & Sons, 1992).

22. H. C. Tsai, H. W. Shiu, M. C. Chuang, C. H. Chen, C. Y. Su, J. D. White, et al., Graphene reduction dynamics unveiled. 2D Materials 2 (2015), 031003.

23. Y. Z. Hong, W. H. Chiang, H. C. Tsai, M. C. Chuang, Y. C. Kuo, L. Y. Chang, et al, Local oxidation and reduction of graphene. Nanotechnol. 28 (2017), 395704.

24. A. Johansson, H.-C. Tsai, J. Aumanen, J. Koivistoinen, P. Myllyperkiö, Y.-Z. Hung, et al., Chemical composition of two-photon oxidized graphene. Carbon 115 (2017), 77-82.

25. Y. Matsumoto, M. Koinuma, S. Y. Kim, Y. Watanabe, T. Taniguchi, K. Hatakeyama, et al., Simple photoreduction of graphene oxide nanosheet under mild conditions. ACS Appl. Mater. Interfaces 2 (2010), 3461-6.

26. S. Prezioso, F. Perrozzi, M. Donarelli, E. Stagnini, E. Treossi, V. Palermo, et al., Dose and wavelength dependent study of graphene oxide photoreduction with VUV Synchrotron radiation. Carbon 79 (2014), 478-85.

27. R. Larciprete, S. Fabris, T. Sun, P. Lacovig, A. Baraldi, S. Lizzit, Dual path mechanism in the thermal reduction of graphene oxide. J. Am. Chem. Soc. 133 (2011), 17315-17321.

CAPTIONS

FIG. 1: (a) The SPL patterns, (b) the 2-PO patterns, (divided by a red dashed line). The optical, frictional and chemical properties of oxidized graphene patterns are showed in the OM, LFM and SPEM images, respectively (from left to right).

FIG. 2: Contour plot/waterfall plot of the in-situ acquired XPS (a)/(b) category A: SPL $|V_{bias}|$ = 8 V; (c)/(d) category B: SPL $|V_{bias}|$ = 10 V, (e)/(f) category C: 2-PO T_{ox} = 1.0 s/spot.

FIG. 3: Fitted XPS (marked by TOC and $C_{epoxy+ether}$) and time evolution of the functional groups during x-ray induced reduction of oxidized graphene prepared by (a) SPL $|V_{bias}|$ = 10 V on Graphenea graphene, TOC = 70.7 % (b) 2-PO T_{ox} = 0.6 s/spot on Graphenea graphene, TOC = 68.5 %, (c) SPL $|V_{bias}|$ = 10 V on RTCVD grown graphene, TOC = 89.7 %, (d) 2-PO T_{ox} = 1.0 s/spot on Graphenea graphene, TOC = 88.6 %.

FIG. 4: Correlation diagram of redox/no redox with respect to TOC vs. concentration of (a) carbon network bonds (C-C+ C=C), (b) functional groups with lower binding energy (epoxy+ether+hydroxyl) (B.E. < 287 eV), (c) functional groups with higher binding energy (carbonyl+carboxyl) (B. E. > 287 eV), and (d) epoxy+ether.

FIG. 5 (a) Correlation diagram of final $C_{C-C+C=C}$ to $C_{epoxy+ether}$. (b) Correlation diagram of final $C_{C-C+C=C}$ to TOC. (c) Schematic diagram showing the physical pictures of the reduction-oxidation processes.

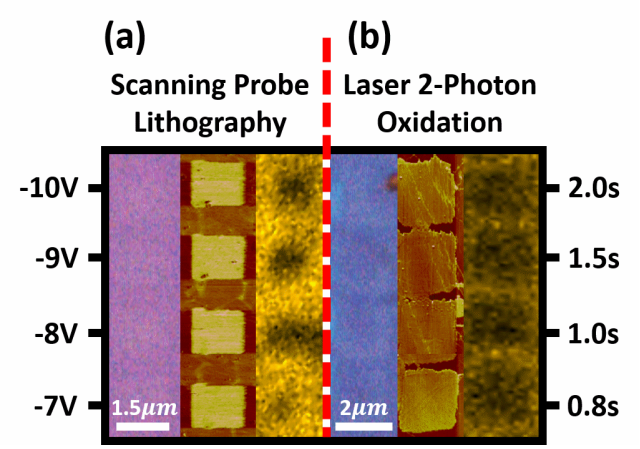

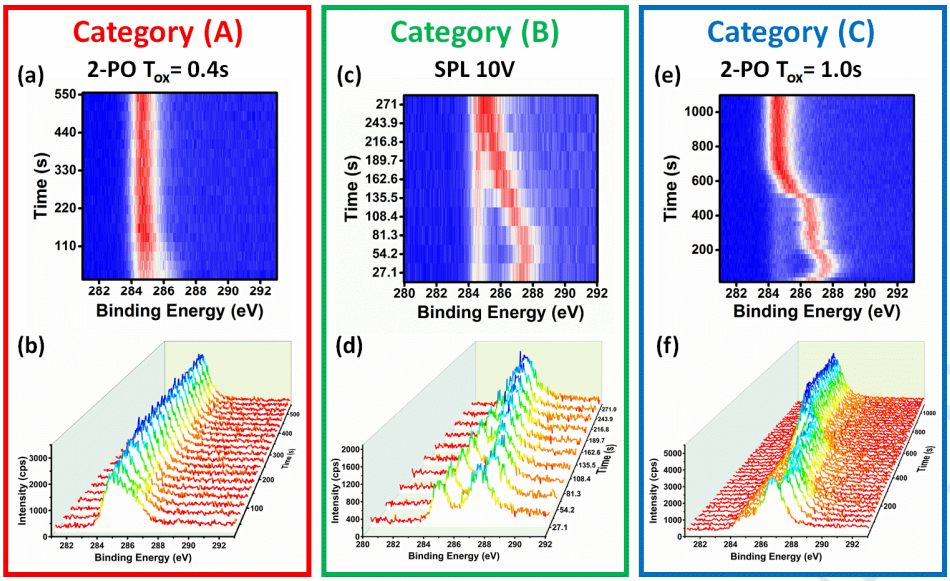

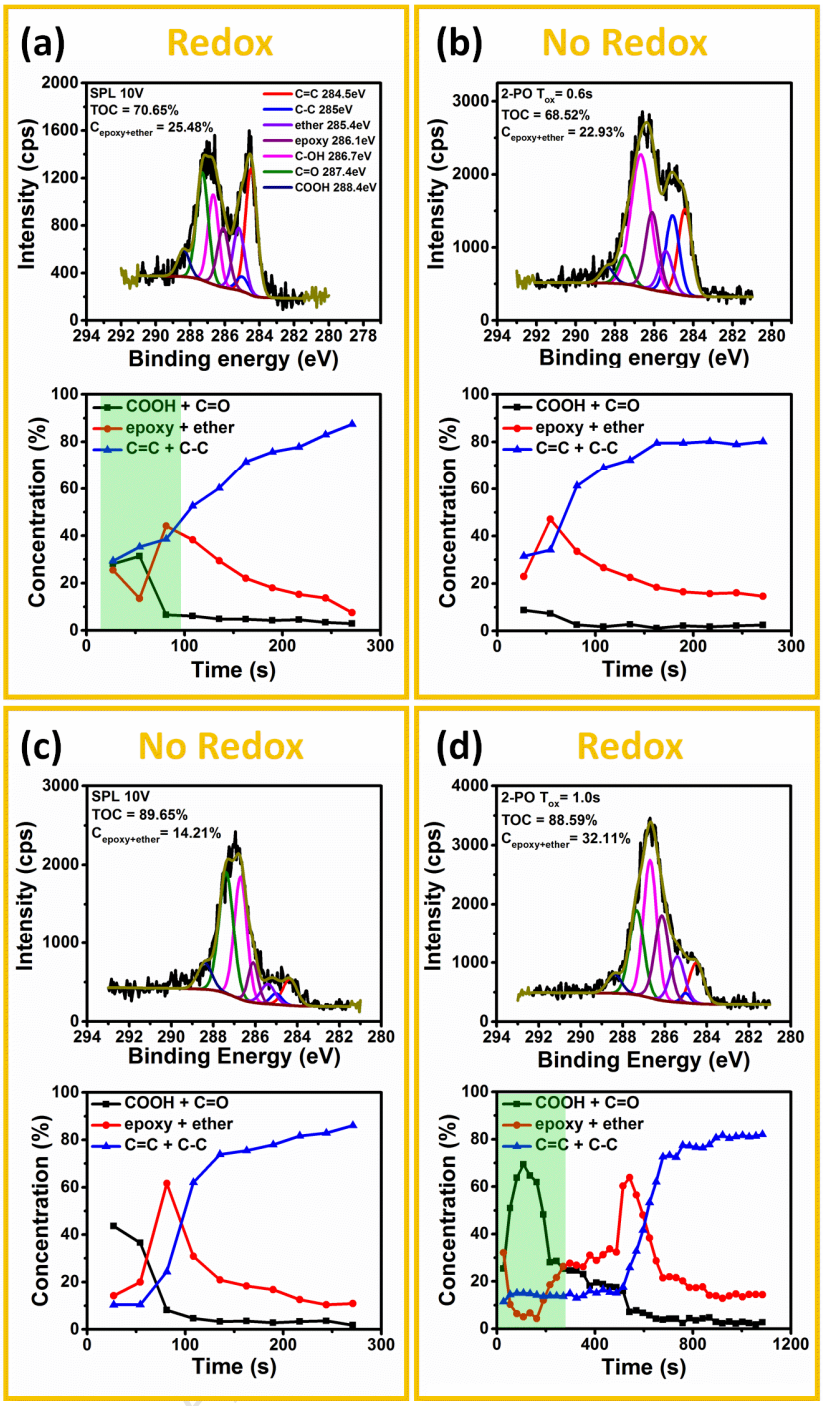
(a)
Redox
SPL 10V
TOC = 70.65%
C_epoxy+ether = 25.48%
C=C 284.5eV
C-C 285eV
ether 285.4eV
epoxy 286.1eV
C-OH 286.7eV
C=O 287.4eV
COOH 288.4eV
Intensity (cps)
Binding energy (eV)
COOH + C=O
epoxy + ether
C=C + C-C
Concentration (%)
Time (s)
(b)
No Redox
2-PO T_ox = 0.6s
TOC = 68.52%
C_epoxy+ether = 22.93%
Intensity (cps)
Binding energy (eV)
COOH + C=O
epoxy + ether
C=C + C-C
Concentration (%)
Time (s)
(c)
No Redox
SPL 10V
TOC = 89.65%
C_epoxy+ether = 14.21%
Intensity (cps)
Binding Energy (eV)
COOH + C=O
epoxy + ether
C=C + C-C
Concentration (%)
Time (s)
(d)
Redox
2-PO T_ox = 1.0s
TOC = 88.59%
C_epoxy+ether = 32.11%
Intensity (cps)
Binding Energy (eV)
COOH + C=O
epoxy + ether
C=C + C-C
Concentration (%)
Time (s)